International Journal of Nanomedicine

Dovepress

open access to scientific and medical research

Open Access Full Text Article

ORIGINAL RESEARCH

Key Modulation of ROS and HSP for Effective Therapy Against Hypoxic Tumor with Multifunctional Nanosystem

Bangzhen Ma[1,2], Yisheng Zhao[3], Xiaoli Liu[4], Mengping Huo[2], Jinghong Wang[2], Jiwei Ma[2], Yang Zhang[2], Chengkun Qin[1,2]

[1]Shandong Provincial Hospital, Shandong University, Jinan, Shandong, 250021, People's Republic of China; [2]Shandong Provincial Hospital Affiliated to Shandong First Medical University, Jinan, Shandong, 250021, People's Republic of China; [3]School of Pharmaceutical Sciences, Key Laboratory for Natural Active Pharmaceutical Constituents Research in Universities of Shandong Province, Shandong Analysis and Test Center, Qilu University of Technology (Shandong Academy of Sciences), Jinan, Shandong, 250353, People's Republic of China; [4]Department of Hernia and Abdominal Wall Surgery, Beijing Chaoyang Hospital, Capital Medical University, Beijing, 100043, People's Republic of China

Correspondence: Chengkun Qin; Yang Zhang, Shandong Provincial Hospital, 324 Jingwu Road, Huaiyin District, Jinan City, Shandong Province, People's Republic of China, Email qinchengkun_slyy@163.com; zhangyang@sdfmu.edu.cn

Background: Though nanomedicine-based photothermal therapy (PTT) has demonstrated promising prospect in tumor treatment due to its high therapeutic efficiency and controllable range, the overexpression of heat shock proteins (HSPs) during PTT can lead to intracellular thermal resistance and reduce its effectiveness. Reactive oxygen species (ROS), followed by the application of chemodynamic therapy (CDT) and photodynamic therapy (PDT), can eliminate HSPs and overcome thermal resistance. However, the tumor microenvironment, including hypoxia and glutathione (GSH) overexpression, impedes the production of ROS and therapeutic efficacy of CDT and PDT. Therefore, we proposed a multifunctional nanoplatform (HMPB@TCPP-Cu) driving PTT/ PDT/ CDT synergistic therapy for tumor treatment via modulating ROS and HSPs.

Methods and Results: In this work, a novel nanoplatform (HMPB@TCPP-Cu) composed of O_2/PTT supplier HMPB (hollow mesoporous Prussian blue) and the loaded PDT/CDT agent (TCPP-Cu^{2+}) was prepared. HMPB acts as an photothermal converter, effectively raising the tumor temperature and inducing apoptosis. HMPB is also a potent catalase-like nanozyme, which can catalyze hydrogen peroxide into oxygen and reduce tumor hypoxia, thus elevating the efficiency of ROS production and the effectiveness of PDT with the wing of sonosensitizer-TCPP. The intracellular glutathione(GSH) was depleted by Cu^{2+} and •OH was generated along with the Cu^{2+}/Cu^{+} converting and Cu^{+}-mediated Fenton-like reaction. Subsequently, the increased levels of ROS effectively eliminate intratumoral thermal resistance. The HMPB@TCPP-Cu has achieved synergistic PTT/PDT/CDT for hepatoblastoma treatment and significant inhibition of tumor growth was detected both in vitro and in vivo.

Conclusion: This study presents a multifunctional nanoplatform that combines photothermal/ chemodynamic/ photodynamic therapy for efficient hepatoblastoma treatment via modulating ROS and HSPs. Collectively, this study provides an appealing strategy in the cleavage of thermal resistance and a novel assistance and enhancement on thermal-related therapies.

Keywords: photothermal therapy, heat shock protein, reactive oxygen species, photodynamic therapy, chemodynamic therapy

Introduction

Hepatoblastoma is a common tumor of the liver in children with high malignance and short survival time. The current status of treatment for hepatoblastoma is not optimistic.[1,2] When tumors are detected, they are mostly already locally advanced, and removing them all at once is challenging. As an emerging yet effective treatment modality, PTT has played a critical role in comprehensively treating various malignant tumors.[3] PTT can convert laser energy into heat and elevate the temperature of tumor tissues with the aid of photothermal converters, thus inducing apoptosis in tumor cells. It has been shown that tumor cells are more sensitive to thermal stimulation than normal cells. When the temperature of tumor cells reaches 40–48 °C, significant apoptosis is detected in tumor cells rather than normal ones spatio-temporally.

Received: 23 August 2023
Accepted: 9 November 2023
Published: 18 November 2023

However, under such circumstance during PTT, heat shock proteins are over-expressed, thus inducing thermal resistance and reducing the efficacy of photothermal therapy.[4,5]

The removal of thermal resistance in tumors is of great significance in improving the effectiveness of photothermal therapy. Many studies have been aiming at the cleavage of thermal resistance and the production of ROS, which are produced from PDT and CDT, playing an important role in this progress.[6–8] The expression of HSPs in tumor cells can be effectively regulated by ROS, and at the same time, ROS can promote the cleavage of HSPs in tumor cells, thus regulating the content of HSPs and reducing thermal resistance during PTT. PDT uses photosensitizers that can convert intracellular oxygen into singlet oxygen under laser irradiation.[9,10] CDT produces ROS in tumor cells through Fenton or Fenton-like reactions, inducing apoptosis in tumor cells and thereby inhibiting tumor growth.[11]

Though identified with preferable ability in producing ROS, the effectiveness of PDT and CDT are limited by the special tumor microenvironment (tumor hypoxia and high glutathione content).[12–15] Because of the limited oxygen levels within solid tumors, it has been shown that insufficient oxygen supply under optical irradiation significantly affects the efficacy of PDT, limiting ROS production and increasing tumor resistance to most standard treatment modalities. Furthermore, PDT consumes large amounts of tissue oxygen to generate ROS, thus enhancing hypoxia, which conversely leads to a greater reduction in the effectiveness of this modality. To improve the effectiveness of PDT, many studies are being conducted to adjust the tumor microenvironment, increase the oxygen content of tumor tissue, and decrease the metabolism of ROS.[16,17] Glutathione (GSH) overexpression in tumor cells can reduces the intracellular ROS levels, leading to limited therapeutic efficacy.[11,18–20] Therefore, reduction of GSH content will increase the effect of ROS production. Researchers applied transition metals to intervene in GSH depletion, such as Mn^{4+} and Cu^{2+}, thus enhancing the ROS yielding and improving the therapeutic efficiency.[21]

Herein, we propose a synergistic nanosystem (HMPB@TCPP-Cu) containing Prussian blue (PB), TCPP (Tetrakis (4-carboxyphenyl) porphyrin), and Cu^{2+}, achieving the synergistic photothermal, photodynamic, and chemodynamic therapy of tumor. Prussian blue is a kind of photothermal converter, which can generate heat under laser irradiation to achieve PTT. It also is a promising nanozyme with catalase-like activity, which can catalyze hydrogen peroxide into oxygen and reduce tumor hypoxia, thus elevating the efficiency of ROS production and the effectiveness of PDT[22,23] with the wing of TCPP. Concerning the CDT agent, the introduction of Cu^{2+} make GSH depletion and CDT feasible. The low redox potential of Cu^{+}/Cu^{2+} can effectively deplete GSH in tumor cells and prevent the GSH-induced destruction of nascent ROS. Meanwhile, Cu^{1+} can generate ROS through CDT.[24,25] The co-produced ROS derived from PDT and CDT can suppress the amount of heat shock proteins, thereby reducing the thermal resistance to PTT.[26–28] This nanosystem HMPB@TCPP-Cu simultaneously overcomes the drawbacks of PTT, PDT and CDT, and reveals the synergistic effect of these modalities.

Materials and Methods

All reagents are commercially available and can be used without any treatment. TCPP-Cu^{2+} was purchased from Wohler Organic (Chongqing, China), PVP (K30, polyvinylpyrrolidone) and potassium ferricyanide ($K_3[Fe(CN)_6]$) were purchased from Adamas (Shanghai, China), hydrogen peroxide, hydrochloric acid, ethanol and acetone were purchased from Sinopharm Chemical Reagent (Shanghai, China); Cell Counting Kit-8 was purchased from MCE (MedChemExpress (United States)); TMB Kit purchased from Beyotime (Shanghai, China); Glutathione Reductase Kit with DTNB purchased from Beyotime (Shanghai, China); Calcein AM/PI Double Stain Kit purchased from MaoKang Biologicals (Shanghai, China); PI/Annexin V Apoptosis Detection Kit purchased from BD Pharmingen (United States).

Preparation of Hollow Mesoporous Prussian Blue

Hollow mesoporous Prussian blue nanoparticles were prepared using the defect-selective etching method. First, the PVP (5.0 g), $K_3[Fe(CN)_6]$,(396 mg) and HCl (1M, 40mL) solutions were mixed thoroughly using a magnetic stirrer to obtain a clear yellow solution, then the reaction vessel was placed in an oven at a set temperature of 80 °C for 24 h. After cooling at room temperature (22 °C −24 °C), the same volume of acetone solution was added, ultrasonically dispersed for 30 min, and centrifuged at 13,000 rpm for 30 min. Then, the PB was obtained by washing with ethanol and double-distilled water and centrifuged, respectively, and the procedure was repeated three times. The above nanoparticles were preserved in 40 mL of ultrapure water.

20 mL HCl with a fixed concentration of 6 M and 20 mL of the above Prussian blue solution were added into a glass vessel and mixed thoroughly using a magnetic stirrer. The products were purified with ultra-pure water by centrifugation for three times and stored at 4 °C.

Preparation of HMPB@TCPP-Cu

Prussian blue nanoparticles have a large pore structure, making the loading of TCPP-Cu possible. First, 10 mg of TCPP-Cu^{2+} was added to 10 mL of DMF to prepare a TCPP-Cu^{2+} solution. To load TCPP-Cu^{2+} on HMPB, the TCPP-Cu^{2+} solution (1mL, 1mg) was added to the HMPB solution (10mg) and magnetic stirred continuously for 4 h at room temperature (22°C–24°C). Subsequently, to remove the unbound TCPP-Cu^{2+}, the prepared HMPB@TCPP-Cu was washed several times using double-distilled water and centrifuged at 13,000 rpm for 30 min. HMPB@TCPP-Cu was dissolved in 5 mL of ultrapure water and stored away from light.

Characterization of HMPB and HMPB@TCPP-Cu

Electron microscopy images were obtained using a transmission electron microscope (TEM, LIBRA 200 CS, Carl Zeiss Co., Germany) and a scanning electron microscope (SEM, Sigma, Carl Zeiss Co.). The BET (Brunauer-Emmett-Teller) method was employed to conduct a particle composite fractionation test in order to investigate the pore structure and specific surface area of HMPB@TCPP-Cu. X-ray diffraction (Rigaku Ultimate IV, Japan) was used to demonstrate the crystallinity of the HMPB@TCPP-Cu. X-ray photoelectron spectroscopy (XPS) (Thermo Scientific K-Alpha, USA) analysis was performed using an ESCALAB 250 X-ray photoelectron spectrometer equipped with a monochromatic X-ray source. Fourier transform-infrared spectra were obtained using a Thermo ls50 instrument (Thermo Scientific, Inc., MA, USA). Dynamic light scattering (Zetasizer Nano Z; Malvern Instruments, Malvern, UK) was used to determine the hydrodynamic particle size distribution and zeta potential of the synthesized nanoparticles.

Oxygen Generation Properties of the Nanoparticles

Oxygen concentrations were measured every 30s using a portable dissolved oxygen meter (WLDO-300, Shanghai Water Instrument Technology Co., Ltd.). The oxygen electrode probe was placed in a reaction system containing HMPB and hydrogen peroxide, where the HMPB concentration was set at 0, 50, 100, 200, and 500 ppm. To ensure consistent experimental conditions, all experiments were performed in a water bath, maintaining the reaction temperature at 37 °C.

Photothermal Characteristics of the HMPB@TCPP-Cu

Evaluation of Temperature Elevation Ability of HMPB@TCPP-Cu

To evaluate the ability of HMPB@TCPP-Cu to raise the temperature of a solution, the temperature rise of the nanomaterial under laser irradiation was recorded using an infrared thermographic camera (Ti32, Fluke) at a rate of 1 frame/second. The infrared thermograms obtained were analyzed using Analyze IR software.

To investigate the temperature increase of the materials under laser irradiation with respect to the concentration, the concentration of HMPB@TCPP-Cu was set to 0, 25, 50, 100, and 200 ppm. Next, 100 μL of the HMPB@TCPP-Cu solutions were placed in a 96-well plate, and the power density of the IR laser was set to 2 W/cm^2. Finally, the temperature increase was recorded and analyzed.

To investigate the correlation between the temperature increase and the laser density, 100 μL aliquots of a 100 ppm HMPB@TCPP-Cu solution were placed in each well of a 96-well plate, and the laser power density was set to 0, 1, 2, and 3 W/cm^2. The temperature increase was then recorded and analyzed.

Evaluation of the Photothermal Conversion Stability of HMPB@TCPP-Cu

To determine the stability of the photothermal conversion of HMPB@TCPP-Cu, 100 μL aliquots of a 100 ppm HMPB@TCPP-Cu solution were placed in each well of a 96-well plate and the laser density set at 2 W/cm^2. Next, six cycles of IR laser irradiation were performed, each for 5 min, and the temperature increase of the nanoparticles under laser irradiation was recorded using an infrared thermographic camera (Ti32, Fluke Inc.) at a rate of 1 frame/second. The infrared thermograms obtained were analyzed using Analyze IR software.

Quantitative Testing of HMPB-Loaded TCPP-Cu

TCPP-Cu solutions were prepared at concentrations of 5, 10, 20, 25, 50, 100, 150, and 200 μg/mL and their absorbance was measured to establish a standard curve. The HMPB@TCPP-Cu materials were synthesized by adding 10 mg of HMPB and 1 mg of TCPP-Cu, which were then stirred overnight and centrifuged to obtain the precipitate. The remaining TCPP-Cu in the supernatant was measured for its absorbance, which was used to quantify the HMPB@TCPP-Cu materials. The results demonstrate a reliable and effective method for quantifying HMPB@TCPP-Cu materials, which may have potential applications in various fields of medicine.

Copper Ion Release Properties of the Nanoparticles

In order to examine the release of copper ions from HMPB@TCPP-Cu, 1 mL of a 2000 ppm HMPB@TCPP-Cu solution was taken and centrifuged at 4000 rpm for 20 min. The sediment obtained via centrifugation was fully redissolved in PBS solutions at pH 5.5, 6.5, and 7.0. Briefly, the solutions were packed in a dialysis bag, and the dialysis bag containing the solution was placed in a 15 mL centrifuge tube and on a shaker during the experimental procedure. Samples were taken at 30-min intervals up to 3 h and then testing copper ion content by ICP-Ms:Agilent 7850.

Photodynamic Characteristics of the Nanoparticles

To verify that the synthesized nanosystem can mediate PDT and generate singlet oxygen species, the experimental group was tested using a SOSG kit with a fluorescence enzyme marker. The PBS group was set as the control group, the concentration of nanodrug in the experimental group was 200 ppm, and the concentrations of hydrogen peroxide were set as 0, 200, 500, and 1000 μM. Laser irradiation at a power of 1 W/cm² was performed for 0, 1, 3, 6, 10, 15, 20, and 30 min.

Chemodynamic Characteristics of the HMPB@TCPP-Cu

To investigate the ability of the synthesized nanomedicine platform to generate hydroxyl radicals, the experimental group was tested using a TMB kit. Meanwhile, the optimal reaction temperature and pH were also determined and experimental data were obtained using a fluorescent enzyme standard.

A consistent reaction system was set up with a HMPB@TCPP-Cu concentration of 200 ppm and a hydrogen peroxide concentration of 500 μM. To explore the optimal reaction pH, the pH was set to 3.0, 4.0, 5.0, and 6.5, and the reaction was carried out in a water bath at 37 °C. To investigate the effect of temperature on hydroxyl radical production, the reaction temperature was set at 30, 37, and 45 °C.

GSH Consumption Properties of the HMPB@TCPP-Cu

To test the ability of the nanodrug to deplete GSH, a 1 mL mixed solution reaction system consisting of GSH and HMPB@TCPP-Cu were prepared. The concentration of GSH was set at 1 mM, while the concentration of HMPB@TCPP-Cu was set at 0, 50, 100, and 200 ppm, and the combinations of the two solutions were allowed to react. At 0, 1, 2, 3, 4, 5, and 6 h, 100 μL of the reaction solution was taken for centrifugation, and the supernatant was collected. Glutathione assay kit (DTNB method) was then added to the supernatant, and its absorbance was measured in an Multiskan SkyHigh Full Wavelength Enzyme Labeler (Thermo Fisher Scientific, USA).

Cell Culture

Human hepatoblastoma HuH6 cells were purchased from the Shanghai Fu Heng Biotechnology Co. (Shanghai, China). DMEM supplemented with 10% fetal bovine serum (FBS), streptomycin (100 μg/mL), and penicillin (100 μg/mL) was used as the culture medium. Cells were cultured at 37 °C in a 5% CO_2 atmosphere. The spent cell culture medium was replenished daily.

Cytotoxicity Studies in vitro

To investigate the in vitro anti-tumor effects of PDT, PTT, CDT, and their synergistic effects, 1×10^5 HuH6 cells were inoculated into each well of a 24-well culture plate containing 600 μL of culture medium. When the cells reached

approximately 70% confluence, the spent cell culture medium was removed, and fresh cell culture medium was added. The cells were then classified according to the planned experimental groups: Group 1, serum-free medium (control); Group 2, TCPP-Cu; Group 3, TCPP-Cu+Laser; Group 4, TCPP+Laser; Group 5, HMPB+Laser; and Group 6, HMPB@TCPP-Cu+Laser. The cells were incubated in a 37 °C incubator for 4 h, then the groups that required laser irradiation were irradiated at a density of 2W/cm^2 for 10 min. Cell viability was measured using a CCK-8 kit to verify the in vitro anti-tumor effect of each treatment. During laser irradiation, the temperature increase of the cell solution was recorded using an infrared thermographic camera (Ti32, Fluke) at a rate of 1 frame/second. The infrared thermograms were analyzed using Analyze IR software to examine the photothermal properties of the nanoparticles that were engulfed into the interior of the cells.

IC-50 Determination of the Nanoparticle Composite HMPB@TCPP-Cu

HuH6 cells (1 million) were first seeded into a 24-well plate until they reached approximately 70% confluency, following which the initial culture medium was removed. Afterwards, the cells were treated with HMPB@TCPP-Cu-enriched culture medium at six different concentrations: 0 ppm, 25 ppm, 50 ppm, 100 ppm, 200 ppm, and 400 ppm. They were then incubated at 37°C for 4 hours in a cell incubator before the culture medium was replaced. The cells were subsequently irradiated with a laser at 2W/cm^2 intensity for 10 minutes. Cell viability was assessed using a CCK-8 assay kit, and the data obtained was used to plot a graph and calculate the IC-50 value.

In vitro Intracellular Uptake Assay

The ability of the synthesized HMPB@TCPP-Cu to enter tumor cells smoothly is a prerequisite for its therapeutic effect. To verify whether it can enter cells, HMPB@TCPP-Cu was combined with the fluorescent agent FITC. HuH6 cells were cultured in 24-well plates and incubated in a 37 °C cell culture incubator for 24 h. The spent medium was then replaced with a fresh medium containing 200 ppm of HMPB@TCPP-Cu, and the entry of nanodrug into the cells was observed via laser confocal microscopy after 1, 2, and 4 h.

Apoptosis Assay Using Cell Viability/Death Staining

To analyze the in vitro anti-tumor effects of PDT, PTT, CDT, and their synergistic effects, the survival and death of HuH6 cells were visualized using CAM/PI double-staining kit and fluorescence microscopy. Briefly, 1×10^5 HuH6 cells were inoculated in each well of a 24-well culture plate containing 600 μL of the culture medium. When the cells reached approximately 70% confluency, the spent cell culture medium was removed, and fresh cell culture medium was added. Laser irradiation was then performed according to the pre-planned experimental groups: Group 1, serum-free medium (control); Group 2, TCPP-Cu; Group 3, TCPP-Cu+Laser; Group 4, TCPP+Laser; Group 5, HMPB+Laser; and Group 6, HMPB@TCPP-Cu+Laser. The cells were incubated in a 37 °C incubator for 4 h, then the groups that required laser irradiation were irradiated at a laser density setting of 2 W/cm^2 for 10 min. Finally, the cells were stained with a Calcein AM/PI double-staining kit for 30 min and analyzed using fluorescence microscopy.

Quantitative Apoptosis Assay

To quantitatively assess the cell apoptosis in each experimental group, 1×10^5 HuH6 cells were inoculated per well of a 24-well cell culture plate containing 600 μL of culture medium. When the cells reached approximately 70% confluence, the spent cell culture medium was removed and fresh cell culture medium was added. Laser irradiation was then performed according to the following experimental groups: Group 1, serum-free medium (control); Group 2, TCPP-Cu; Group 3, TCPP-Cu+Laser; Group 4, TCPP+Laser; Group 5, HMPB+Laser; and Group 6, HMPB-TCPP-Cu+Laser. The cells were incubated at 37 °C incubator for 4 h then the groups that required laser irradiation were irradiated at a laser density setting of 2 W/cm^2 for 10 min. Finally, the cells were stained with a PI/Annexin V Apoptosis Detection Kit and analyzed using flow cytometry.

ROS Production Experiment Based on HuH6 Cells

First, HUH6 cells were cultured in a 24-well plate. Three experimental groups were designed as follows: Group 1, control group; Group 2, HMPB@TCPP-Cu group; Group 3, HMPB@TCPP-Cu+Laser group. When the cell confluence reached approximately 70%, the original cell culture medium was discarded and replaced with HMPB@TCPP-Cu-containing cell culture medium. After 4 hours of incubation, the cell culture medium was replaced as per the experimental design. Laser irradiation was performed on Group 3. Reactive oxygen species (ROS) were stained using a reactive oxygen species detection kit, and the level of ROS production was observed using a fluorescence microscope.

Cytotoxicity Assay of HMPB@TCPP-Cu in Hepatic Stellate Cells

First, LX-2 cells were seeded into a 24-well plate. When the cell confluence reached approximately 70%, the cell culture medium was removed. Then, cell culture medium containing HMPB@TCPP-Cu was added at four different concentrations (0 ppm, 50 ppm, 100 ppm, and 200 ppm), and the cells were cultured for 12 and 24 hours at 37°C. After replacing the cell culture medium, cell viability was measured using a CCK-8 assay kit, and the data were plotted accordingly.

In vivo Anti-Tumor Studies

Establishment of Animal Tumor Models

The human hepatoblastoma cell line HuH6 was stored in liquid nitrogen before use. Forty-eight healthy male BALB/c nude mice (4 weeks old) were purchased from Hangzhou Ziyuan Experimental Animal Technology Co. and housed in the animal husbandry facility of Shandong University Affiliated Provincial Hospital. All animal husbandry and experiments were performed in accordance with the guidelines established by the Institutional Animal Care and Use Committee of the Shandong University Affiliated Provincial Hospital (No. 2022–039).

Next, HuH6 cells were cultured at 37 °C in a cell culture incubator. The cells of the cell culture flasks were suspended with an appropriate amount of trypsin solution (Gibco), the tumor cell suspension was centrifuged at 1000 rpm for 5 min, washed twice with PBS, and then resuspended in PBS. Next, 150 μL of the cell suspension (containing approximately 1×10^6 cells) was injected subcutaneously into the foreleg of the nude mice to establish a transplantation tumor model.

When the size of the tumor reached approximately 150 mm^3, the HuH6 tumor-bearing nude mice were randomly assigned to six groups (n = 8/group): Group 1, PBS; Group 2, TCPP-Cu; Group 3, TCPP-Cu+Laser; Group 4, TCPP +Laser; Group 5, HMPB+Laser; and Group 6, HMPB@TCPP-Cu+Laser. In summary, nude mice belonging to different experimental groups received tail vein injections of 50μL of PBS (control), TCPP, TCPP-Cu, HMPB, or HMPB@TCPP-Cu solution. The concentration of the injected solution was set at 200 ppm for all groups.

Body Weight and Tumor Volume Analysis in Nude Mice

After solution injection and laser irradiation, the tumor volumes and weights of the nude mice were recorded and analyzed within 21 days after treatment. The horizontal and vertical dimensions of the tumors were measured every other day using Vernier calipers. The tumor volume was calculated as follows: volume = (horizontal length × vertical length^2)/2. In addition, the body weights of the nude mice were obtained every other day by weighing them on a scale.

In vivo Photothermal Characteristics of the Nanoparticles

Twenty-four hours after injection, one nude mouse each from groups 1, 5, and 6 was taken and injected intraperitoneally using an anesthetic drug (tribromoethanol, 280 mg/kg) and irradiated with a laser at a density of 2 W/cm² for 10 min. During this procedure, the temperature increase of the tumors under laser irradiation was recorded using an infrared thermographic camera (Ti32, Fluke) at a rate of 1 frame/second. The infrared thermograms were analyzed using Analyze IR software.

Biodistribution of HMPB@TCPP-Cu Nanoparticles

Cy5.5 was combined with the HMPB@TCPP-Cu nanoparticles. When the tumor volume reached 150 mm^3, 50 μL of the Cy5.5-labeled HMPB@TCPP-Cu particles were injected via the tail vein of the nude mice, and whole-animal imaging was performed at predetermined time points using an in vivo imaging system (Lumina XR, Caliper, USA) to detect the fluorescence intensity.

Histological Evaluation

The ability of CDT and PDT to produce ROS was determined by detecting the production of ROS. The ability of each group to produce ROS to inhibit heat shock protein expression was determined by detecting the expression of HSP70, HSP90, and HiF-1α; the apoptotic pathway involved in each treatment group was determined by detecting the expression of caspase-3 and caspase-9. Apoptosis was detected in each group via TUNEL, PCNA, and HE staining to determine the mechanism of cell death in each treatment group.

According to the experimental groups, the corresponding solutions were injected into the mice via the tail vein, and each group was irradiated with a laser on the tumor at a laser density of 2 W/cm^2 for 10 min. Three cycles of tail vein drug injection and laser treatment were performed for each mouse. Thirty minutes after irradiation, one mouse was selected for anesthesia and tumor tissues were taken, frozen, and preserved in liquid nitrogen to detect ROS production. Twenty-four hours after the end of irradiation, nude mice were anesthetized using tribromoethanol, and tumor specimens were collected and fixed in 4% paraformaldehyde for 24 h. The tumor specimens were then paraffin-embedded and sectioned at a thickness of 5 μm for immunofluorescence analysis of HSP70, HSP90, caspase-3, and caspase-9 expression; PCNA and TUNEL staining; and HiF-1α immunohistochemical analysis and HE staining.

Biotoxicity Testing of Materials in vivo

At the end of the experiment, nude mice were anesthetized via intraperitoneal injection with tribromoethanol (280 mg/kg). The liver, spleen, kidneys, heart, and lungs were taken for HE testing to investigate whether the nanoparticles used in the experiment were biologically toxic to nude mice.

Statistical Analysis

Statistical analysis was performed using SPSS 20 software. Error bars indicate the standard error of the mean. A *t*-test was used between groups to analyze the differences.

Results and Discussion

Synthesis and Characterization of HMPB@TCPP-Cu

After the synthesis of HMPB@TCPP-Cu, the morphology of the prepared nanoparticles was observed using TEM, as shown in Figures 1A and S1. The elemental composition of Cu and Fe (Figures 1B and C) and C, N, and O (Figures S2–S4) in HMPB@TCPP-Cu can also be observed via TEM. SEM imaging revealed that the prepared nanoparticles kept the characteristics of HMPB and its porous structure, which is favorable for interacting with TCPP-Cu nanosheets. Using the BET method for analysis, an obvious hysteresis loop caused by capillary condensation can be observed in the desorption isotherm, indicating the presence of mesopores in the nanocomposite. By employing the BJH method to analyze the desorption branch curve, it can be observed that the pore size distribution of the material is concentrated around 21 nm, with an average pore size of 26.8nm (Figures S5 and S6). Moreover, particle size analysis showed that HMPB@TCPP-Cu has good dispersion, with a diameter of approximately 100 nm (Figures 1D and S7). By comparing the obtained XRD spectrum with the standard spectrum, it was confirmed that the prepared nanoparticles were pure Prussian blue ($Fe_4[Fe(CN)_6]_3$), with strong peaks corresponding to crystal planes at 17.4° (200), 24.8° (220), 35.4° (400), and 39.7° (420). The crystallinity of this sample was calculated to be 25.35%, indicating a well-defined crystal structure of HMPB nanoparticles.(Figure 1E). Based on the XPS spectrum, it is evident that the peaks located at binding energies of 708.29 eV and 721.15 eV can be attributed to the Fe2p3/2 and 2p1/2 signals of Fe^{2+} ions, respectively. The peaks at 708.79 eV and 722.59 eV correspond to the Fe^{3+} 2p3/2 and 2p1/2 signals, respectively. Additionally, satellite peaks were observed at 712.79 eV and 725.90 eV.(Figure 1F).

The samples of HMPB and HMPB@TCPP-Cu were subjected to FTIR analysis, and the infrared spectra exhibited distinct changes when HMPB was combined with TCPP-Cu. These changes were attributed to the introduction of the TCPP structure, which overlapped with the spectral bands of HMPB. The absorption peak observed at 1655 cm^{-1} originated from the stretching vibration mode of C=O, which is a characteristic feature of the ester group introduced by TCPP. Additionally, the hydroxyl stretching vibration absorption peak at 3317 cm^{-1} exhibited a significant blue shift to 3435 cm^{-1}, indicating that the binding of TCPP-Cu altered the hydrogen bonding interactions between HMPB molecules. By comparing the spectral curves with

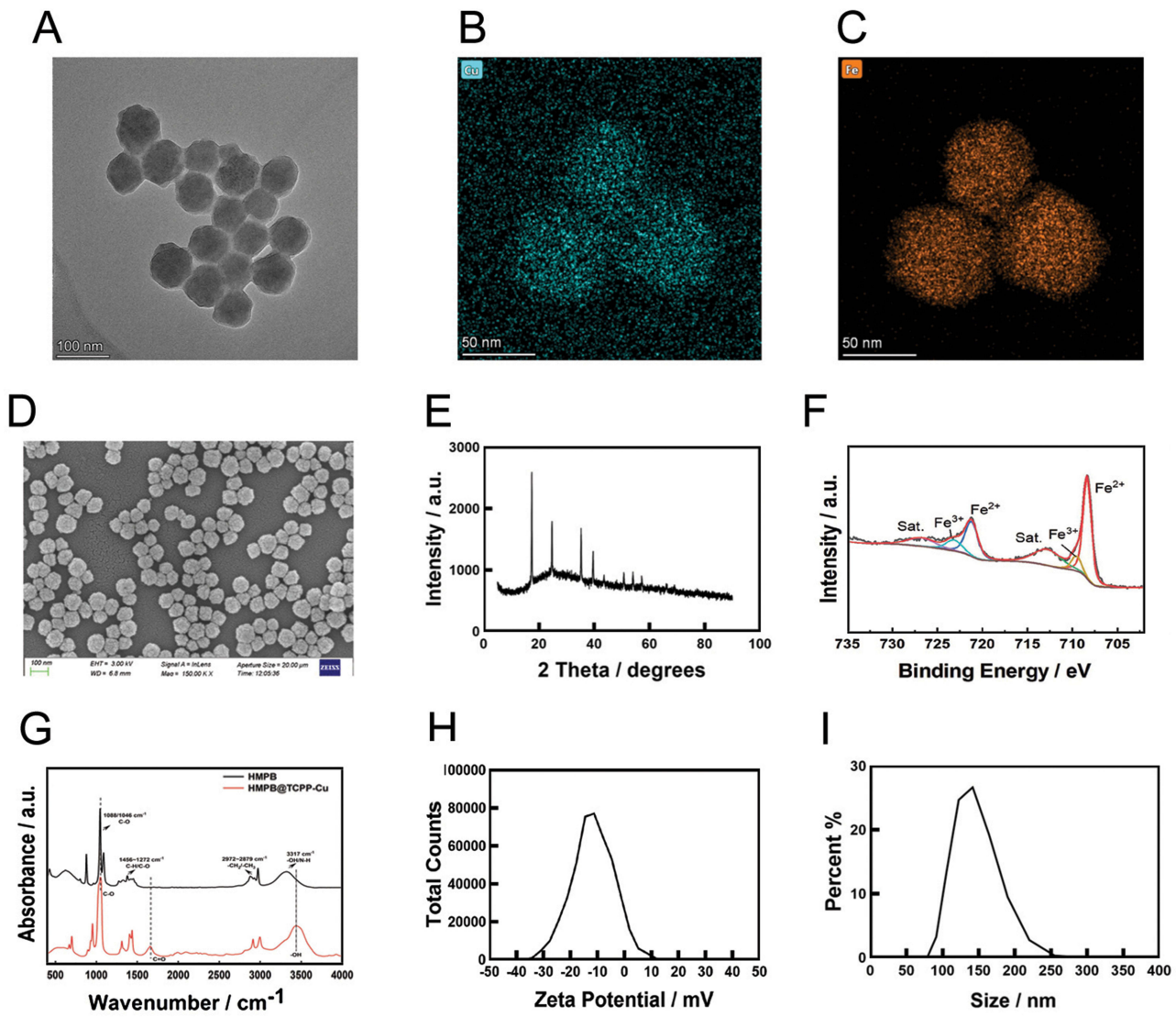

Figure 1 Structural and physicochemical characterization of the HMPB@TCPP-Cu particles. (**A**–**C**) TEM images. (**D**) SEM images. (**E**) XRD of the HMPB@TCPP-Cu particles. (**F**) XPS of the HMPB@TCPP-Cu particles. (**G**) Fourier transform-infrared spectra of the HMPB and HMPB@TCPP-Cu particles. (**H**) Zeta potential of the nanoparticles. (**I**) Particle size distribution of the nanoparticles.

a standard spectrum and conducting a spectral analysis, it can be concluded that TCPP-Cu was successfully loaded on the surface of HMPB, confirming the successful synthesis of the multifunctional nanoplatform drug HMPB@TCPP-Cu in this experimental study. (Figure 1G). The zeta potential of HMPB@TCPP-Cu was also examined, which was mainly in the range of −11.26 mV to −14.54 mV, indicating the particles had good stability in solution (Figure 1H). The hydrodynamic diameters of the prepared materials were also examined, which were mainly in the range of 173.14 ± 81.86 nm (Figure 1I). Based on the above results, HMPB and TCPP-Cu were successfully loaded, and the prepared HMPB@TCPP-Cu was stable in solution.

Oxygen Generation Properties of the Nanoparticles

A portable oxygen solubility detector was used to monitor the numerical changes in oxygen solubility of the HMPB + H_2O_2 solution. Distilled water was used as a control. To evaluate the ability of HMPB to catalyze the decomposition of H_2O_2 to produce O_2, the concentration of HMPB was set to 200 ppm. By adjusting the concentration of H_2O_2, a gradual increase in the solubility of oxygen in the solution was observed; a higher H_2O_2 concentration indicated a higher oxygen solubility (Figure 2A). Meanwhile, in another set of experiments, the concentration of H_2O_2 was fixed at 500 μm, and the concentration of HMPB was gradually increased. The results showed that the solubility of oxygen increased until it reached a peak at approximately 20

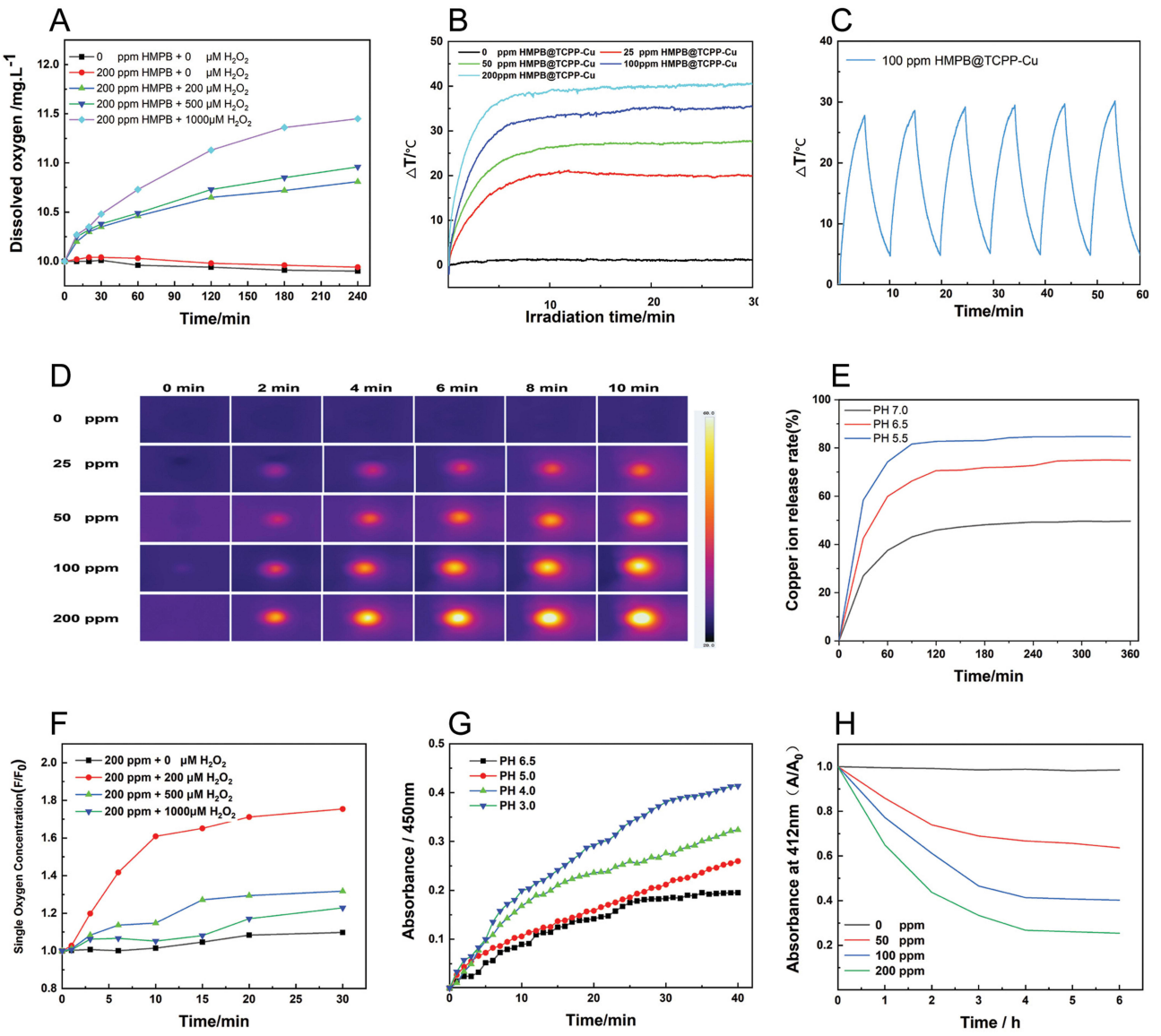

Figure 2 Examination of the performance characteristics of the nanoparticles. (**A**) Curves showing the oxygen concentration with respect to time in an HMPB solution (200 ppm) containing H_2O_2 at concentrations of 0, 200, 500, and 1000 μM. (**B**) Curves of the temperature change with respect to time for an HMPB@TCPP-Cu solution subjected to laser irradiation. The concentration of HMPB@TCPP-Cu was set to 0, 25, 50, 100, and 200 ppm. (**C**) Verification of the photothermal stability of HMPB@TCPP-Cu. The curve shows the change in the temperature of the HMPB@TCPP-Cu solution with time by turning the laser switch on or off every 5 min, with 10 min as one cycle. (**D**) Thermal image of the HMPB@TCPP-Cu solution under laser irradiation when the concentration of HMPB@TCPP-Cu was set to 0, 25, 50, 100, and 200 ppm. (**E**) Copper ion release curves of the HMPB@TCPP-Cu solution at pH 5.5, 6.5, and 7.0. (**F**) Time-course absorbance curves of single-linear state oxygen produced by the reaction of HMPB@TCPP-Cu (0, 200, 500, and 1000 μM) and H_2O_2 (200 ppm) under laser irradiation. (**G**) Absorbance curves of hydroxyl radicals produced by the reaction of HMPB@TCPP-Cu (500 μM) and H_2O_2 (200 ppm) at pH values of 3.0, 4.0, 5.0, and 6.5. The temperature of the reaction system was set to 37 °C. (**H**) Time-course depletion of GSH (1 mM) upon reaction with an HMPB@TCPP-Cu solution (0, 50, 100, and 200 ppm).

min into the reaction (Figure S8). This shows that HMPB has catalase-like activity, which can catalyze the decomposition of H_2O_2 to produce O_2 and increase the solubility of oxygen in water. Since the concentration of H_2O_2 in the tumor microenvironment is higher than that of normal cells, HMPB can be used to catalyze the production of O_2 from H_2O_2, thus providing substrates for the reactions mediated by PDT and CDT.

Photothermal Characteristics of the Nanoparticles

Photothermal Conversion Efficacy

Figure 2B shows the temperature variation of the reaction system with time when the concentrations of HMPB@TCPP-Cu were diluted to 0, 25, 50, 100, and 200 ppm in a 96-well plate, and the power density of the infrared laser was set to 2

W/cm^2; with an increase in the HMPB@TCPP-Cu concentration, the temperature gradually increased, and reached a peak within 10 min. The temperature gradually stabilized thereafter (Figure 2B and D).

Figure S9 shows that the temperature of the reaction solution increased with the increase of laser power density when the concentration of HMPB@TCPP-Cu was diluted to 100 ppm and 100 μL of the solution was placed in a 96-well plate. With an increase in laser power density, the temperature of the reaction solution gradually increased and then stabilized.

Photothermal Stability Experiment

The photothermal stability of HMPB@TCPP-Cu was determined by analyzing the obtained infrared thermograms using Analyze IR software. According to the data, six experimental cycles were conducted, with laser density set at 2 W/cm^2 and each cycle running for 10 min (irradiation for 5 min, and no irradiation for 5 min). The peak temperature reached by the solution in each cycle was similar (Figure 2C). Based on the above experimental results, it was confirmed that HMPB@TCPP-Cu is a relatively stable photothermal conversion agent.

Quantitative Testing of HMPB-Loaded TCPP-Cu

A standard curve was constructed by plotting the absorbance of the solution measured using an enzyme-linked immunosorbent assay reader against the corresponding TCPP-Cu concentrations, as shown in the graph (Figure S10). By measuring the absorbance of the supernatant obtained after the preparation of HMPB@TCPP-Cu and using the standard curve, the mass of TCPP-Cu in the supernatant was calculated, and the loading efficiency of HMPB for TCPP-Cu was determined. The loading efficiency was calculated using the formula: HMPB@TCPP-Cu loading efficiency = (total amount of TCPP-Cu - mass of TCPP-Cu in the supernatant) / (total amount of TCPP-Cu) × 100%. The calculated loading efficiency was 26.35%.

Copper Ion Release Properties of the Nanoparticles

The copper ion contents of the samples taken during the experiment were measured using an ICP-OES:Thermo Fisher iCAP PRO. The copper ion release rate of the nanoparticles in solution was then calculated. Based on the experimental results, the release rate of copper ions gradually increased with time, with a good final release rate effect, providing strong supporting evidence for the use of the fabricated nanoparticles in CDT (Figure 2E). The smooth release of copper ions from the synthesized multifunctional nanomaterial HMPB@TCPP-Cu is a prerequisite for CDT to produce ROS and act as a therapeutic agent for tumors. The results of this experiment confirm that the release of copper ions from HMPB@TCPP-Cu leads to an ideal CDT.

Photodynamic Characteristics of the Nanoparticles

Based on the efficient oxygen generation, the photodynamic effect of the as-synthesized HMPB@TCPP-Cu was carefully analyzed by evaluating their corresponding singlet oxygen generation capacities using the commercial detection probe SOSG. Compared with HMPB@TCPP-Cu and degassed water, HMPB@TCPP-Cu mixed with hydrogen peroxide showed a markedly enhanced singlet oxygen generation ability when exposed to laser irradiation for 0, 1, 3, 6, 10, 15, 20, and 30 min. This apparent enhancement in the ability of HMPB@TCPP-Cu to produce singlet oxygen may be due to the increased oxygen concentration and the presence of photosensitizers (Figure 2F). HMPB@TCPP-Cu generates singlet oxygen via photodynamic therapy under laser light using the oxygen available within the reaction system. A time-dependent measurement of the singlet oxygen concentration was performed using a Fluorescence Enzyme Labeler for 30 min, and the fluorescence spectrum was recorded. Taken together, these results demonstrated that HMPB@TCPP-Cu could effectively generate singlet oxygen under light irradiation and serve as an efficient photodynamic agent for the treatment of cancer.

Chemodynamic Characteristics of the Nanoparticles

The ability of the synthesized HMPB@TCPP-Cu to generate hydroxyl radicals was investigated to explore the optimal reaction temperature and the optimum reaction PH.

Temperature Optimization

Different reaction temperatures were set: 30, 37, and 45 °C. The hydroxyl radical content generated in the reaction system with fixed concentrations of nanoparticles and hydrogen peroxide was measured using a commercially available TMB hydroxyl radical detection kit. It was found that the highest hydroxyl radical content was generated at 45 °C (Figure S11). Therefore, the ability of the reaction system to generate hydroxyl radicals was enhanced with an increase in temperature, but only within a certain range.

pH Optimization

Reactions with different pH values were set (3.0, 4.0, 5.0, and 6.5), and the hydroxyl radical content generated in each reaction system containing fixed concentrations of nanoparticles and hydrogen peroxide was measured using a commercially available TMB hydroxyl radical detection kit. It was found that the amount of hydroxyl radicals generated was the highest at a pH of 3.0 (Figure 2G). This shows that the acidic tumor microenvironment is conducive to the production of ROS, which induces apoptosis in tumor cells.

GSH Consumption Properties of the Nanoparticles

The reaction system was prepared with 1 mL of a mixed solution reaction system consisting of GSH and HMPB@TCPP-Cu, where the concentration of GSH was set to 1 mM, and the concentrations of HMPB@TCPP-Cu were 0, 50, 100, and 200 ppm. After centrifuging each reaction solution, the supernatant was collected, and a Glutathione assay kit (DTNB method) reagent was added for detecting the absorbance in an Multiskan SkyHigh Full Wavelength Enzyme Labeler. The absorbance values (at 412 nm) were measured at six time points, and the results showed that HMPB@TCPP-Cu could catalytically reduce the amount of GSH in a time-dependent manner (Figure 2H).

Cytotoxicity Studies in vitro

Cell viability was detected using the CCK-8 assay, and the PBS-treated group without laser irradiation served as a control. Compared with the control group, the cell viability of all experimental groups was lower, with the HMPB@TCPP-Cu+ Laser group having the lowest cell viability (Figure 3A). Thus, the PDT, PTT, and CDT effects studied in this project were proven to be effective in tumor cell killing and had a synergistic effect with each other. The photothermal performance of HMPB@TCPP-Cu was also determined by analyzing the obtained infrared thermograms using Analyze IR software. The temperatures of the cell cultures in Groups 5 and 6 showed a significant increase upon laser irradiation, with a similar trend of temperature increase observed in both groups. The maximum temperature (approximately 45 °C) was achieved at 15 min, similar to the levels reached during PTT (Figures 3B and S12).

IC-50 Determination of the Nanoparticle Composite HMPB@TCPP-Cu

The IC-50 value, which represents the half-maximal inhibitory concentration, is a commonly used pharmacological parameter for evaluating the extent of inhibition of HMPB@TCPP-Cu on HuH6 cell viability. It provides a quantitative measure for the inhibitory effect of HMPB@TCPP-Cu on tumor cells. Based on the data obtained from the CCK-8 assay kit, the IC-50 value was calculated to be 100.5 ppm (Figure S13), indicating a strong inhibition effect of HMPB@TCPP-Cu on tumor cells. This finding suggests that HMPB@TCPP-Cu has a promising antitumor potential.

In vitro Intracellular Uptake Studies

To verify whether the synthesized nanoparticles can enter cells to exert therapeutic effects, HMPB@TCPP-Cu was mixed into complete DMEM, and this culture medium was used to culture HuH6 cells for 1, 2, and 4 h. Observation using confocal microscopy showed that the material could enter the cytoplasm and that the nanoparticles which were swallowed into the cell gradually increased with time (Figure S14). These results show that the newly synthesized multifunctional nanomaterial HMPB@TCPP-Cu can be phagocytosed by cells and be useful as an anti-tumor therapy.

In addition, this is the first investigation of the cytotoxicity of HMPB@TCPP-Cu nanoparticles in HuH6 cells. The results showed that the nanoparticles were not cytotoxic to HuH6 cells.

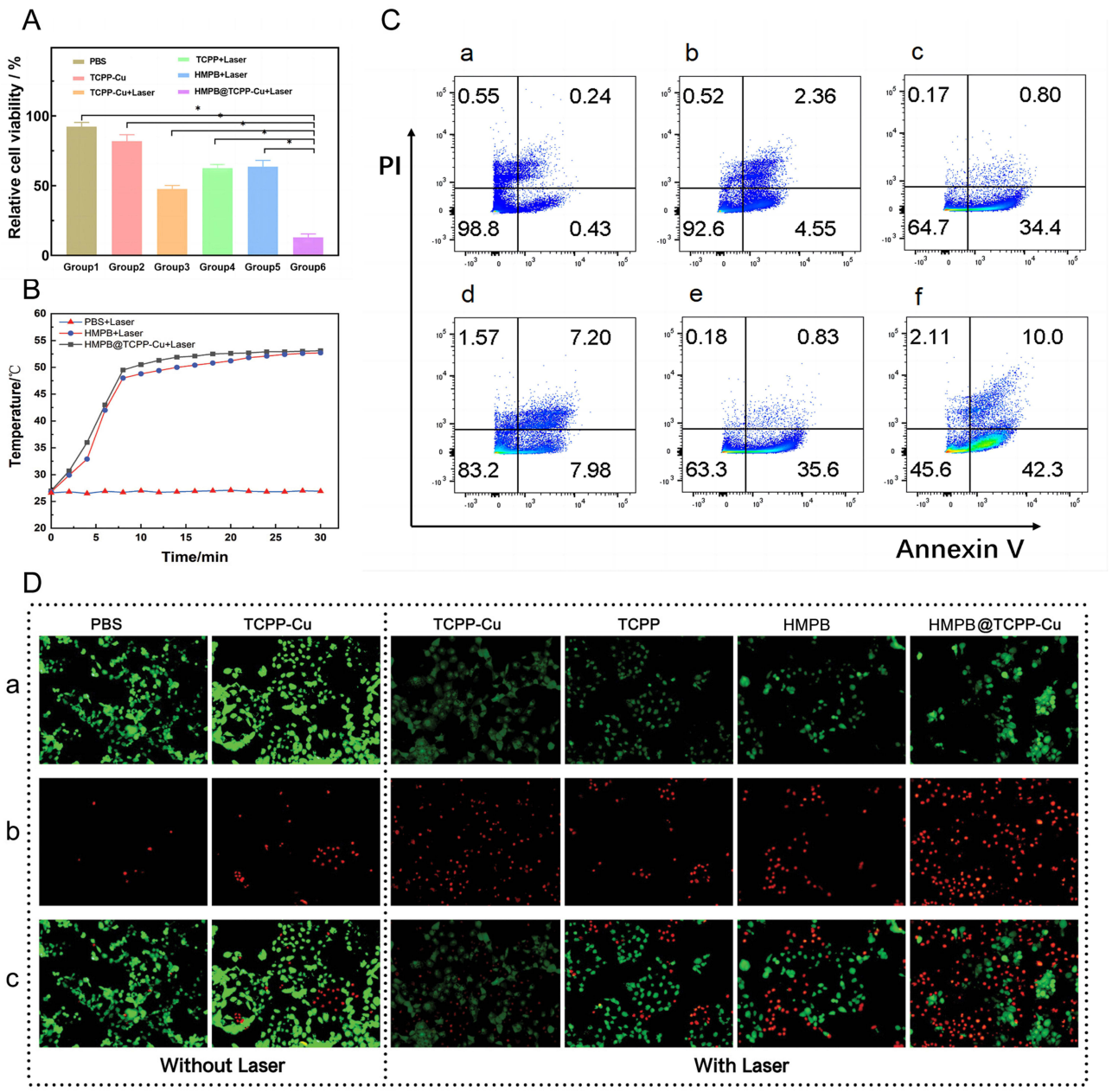

Figure 3 Examination of the anti-tumor properties of the synthesized nanoparticles against hepatoblastoma HuH6 cells. (**A**) Measurement of cell activity in each experimental group. (**B**) A curve showing the variation of the solution temperature with time in a Petri dish incubated with HuH6 cells and subjected to laser irradiation. (**C**) Quantitative analysis of cell apoptosis rates after Annexin V/PI staining of HuH6 cells from each experimental group. (**D**) HuH6 cell survival status analysis in each experimental group after CAM/PI staining.

Apoptosis Assay

The anti-tumor effect of the various treatments employed in this study could be evaluated by observing the survival of tumor cells in each group after being double-stained with Calcein AM /PI and observed using fluorescence microscopy. The tumor cells in Group 6, which were treated with HMPB@TCPP-Cu+Laser, typically showed an apoptotic state and had significantly more apoptotic cells than the other groups. Meanwhile, the tumor cells of Group 1 (PBS-treated) were in a surviving state. In addition, the number of apoptotic tumor cells in all the other groups was significantly more than that of the control group (Figure 3D). This result shows that PTT, PDT, and CDT effectively and efficiently mediated the apoptosis of tumor cells.

Quantitative Apoptosis Assay

To quantitatively assess the apoptosis of HuH6 cells in each experimental group, we used a PI/Annexin V Apoptosis Detection Kit and subjected them to flow cytometry. In the control group (Group 1), only 0.67% were apoptotic, indicating that the cells were in a good growth state. The apoptosis rates in Groups 2–5 were 6.91%, 35.2%, 15.18%, and 36.43%, respectively, showing relatively more evident apoptosis after treatment. The apoptosis rate of the cells in Group 6 reached as high as 52.3% after treatment, indicating that the therapy in this study has a good ability to induce apoptosis in tumor cells, confirming its effect of inhibiting tumor cell growth (Figures 3C and S15).

ROS Production Experiment Based on HuH6 Cells

By using a reactive oxygen species detection kit to stain the cells in the three experimental groups and observing the fluorescence intensity of ROS under a fluorescence microscope, it can be observed that the Control Group exhibits the weakest fluorescence intensity, the HMPB@TCPP-Cu+Laser group exhibits the strongest fluorescence intensity, and the HMPB@TCPP-Cu group exhibits an intermediate fluorescence intensity (Figure S16). This indicates that the combination therapy of PTT, PDT, and CDT represented by HMPB@TCPP-Cu+Laser generates the highest level of ROS, resulting in the strongest inhibitory effect on tumor cells.

Cytotoxicity Assay of HMPB@TCPP-Cu in Hepatic Stellate Cells

The solutions of the experimental groups with concentrations set at 0 ppm, 50 ppm, 100 ppm, and 200 ppm were subjected to absorbance measurements using an enzyme-linked immunosorbent assay (ELISA) reader. Based on the results, no significant differences were observed in cell viability among the experimental groups, indicating that HMPB@TCPP-Cu demonstrates good target specificity and biocompatibility (Figure S17).

The efficacy of the treatment used in this study mainly comes from two aspects: first, the PTT can increase the tumor temperature and exert its anti-tumor activity; second, the nanoparticles entering the cells can generate ROS, enhancing the cellular oxidative stress response, and achieving the effect of PDT and CDT. Moreover, in this system, the effects of OTT, PDT, and CDT are not a simple "1 + 1 + 1" additive combination; in fact, they can promote each other and amplify their individual therapeutic effects.

In vivo Anti-Tumor Studies

In vivo Anti-Cancer Efficacy of HMPB@TCPP-Cu as a Combination of PTT, PDT, and CDT

After their tumors reached approximately 150 mm^3 in size, nude mice with HuH6 tumors were randomly assigned to six groups (n = 8/group) and injected through their tail vein with 50 μL of the following treatments: PBS (control), HMPB, TCPP, TCPP-Cu, or HMPB@TCPP-Cu (Group 1: PBS; Group 2: TCPP-Cu; Group 3: TCPP-Cu+Laser; Group 4: TCPP +Laser; Group 5: HMPB+Laser; Group 6: HMPB@TCPP-Cu+Laser). The concentrations of the injected solutions were set at 200 ppm. At 24 h after drug injection, the animals in each group were anesthetized and subjected to laser irradiation treatment at a laser power density of 2 W/cm^2. The animal experiment was conducted at Laboratory Animal Research Center of Shandong Provincial Hospital with approval by the Animal Care and Use Committee of Shandong Provincial Hospital (No. 2022–039). In the process of animal experimentation, strict adherence to the "3R" principles, which advocate Replacement, Reduction, and Refinement, should be strictly followed. Moreover, it is essential to guarantee the five freedoms that experimental animals are entitled to. These freedoms encompass the absence of hunger and thirst, the absence of discomfort and disease, the ability to exhibit natural behavior, and the absence of fear and distress.

Changes in the Body Weight and Tumor Volume in Nude Mice

We also examined the therapeutic effects of the fabricated nanocatalysts in vivo. To this end, the tumor volume was monitored over 21 days following the administration of the different treatments. The mice in the Group 2, Group 4 and Group 5 exhibited smaller tumor growth than the PBS-treated control group, indicating that PTT, PDT, and CDT can all inhibit tumor growth.

The mice in Group 3 (TCPP-Cu+Laser treatment) exhibited reduced tumor growth compared to those in Groups 1, 2, and 4, indicating that PDT combined with CDT is superior to PDT or CDT alone. Notably, the mice in the HMPB@TCPP-Cu+Laser

group (Group 6) had the smallest tumor volumes compared to all other groups (Figures 4A, E, and S18). These results demonstrate that treatment with HMPB@TCPP-Cu+Laser exhibited the most effective tumor growth suppression, which was attributed to the synergistic combination of PTT, PDT, and CDT.

During the experiment, body weight measurements for each group of animals were taken every other day. At the end of the experiment, no statistical difference was found between the weights of the animals across groups and the changes in the weight of the animals in each group (Figure 4B). This shows that HMPB@TCPP-Cu has no significant toxic effects on the animals.

In vivo Photothermal Characteristics of the Nanoparticles

To estimate the photothermal effect of HMPB@TCPP-Cu on HuH6 tumor-bearing mice, changes in the tumor temperature were recorded over time using a far infrared thermal camera. The maximum tumor temperature in the HMPB+Laser and HMPB@TCPP-Cu+Laser groups increased rapidly and reached nearly 43 °C, which is within the temperature range for

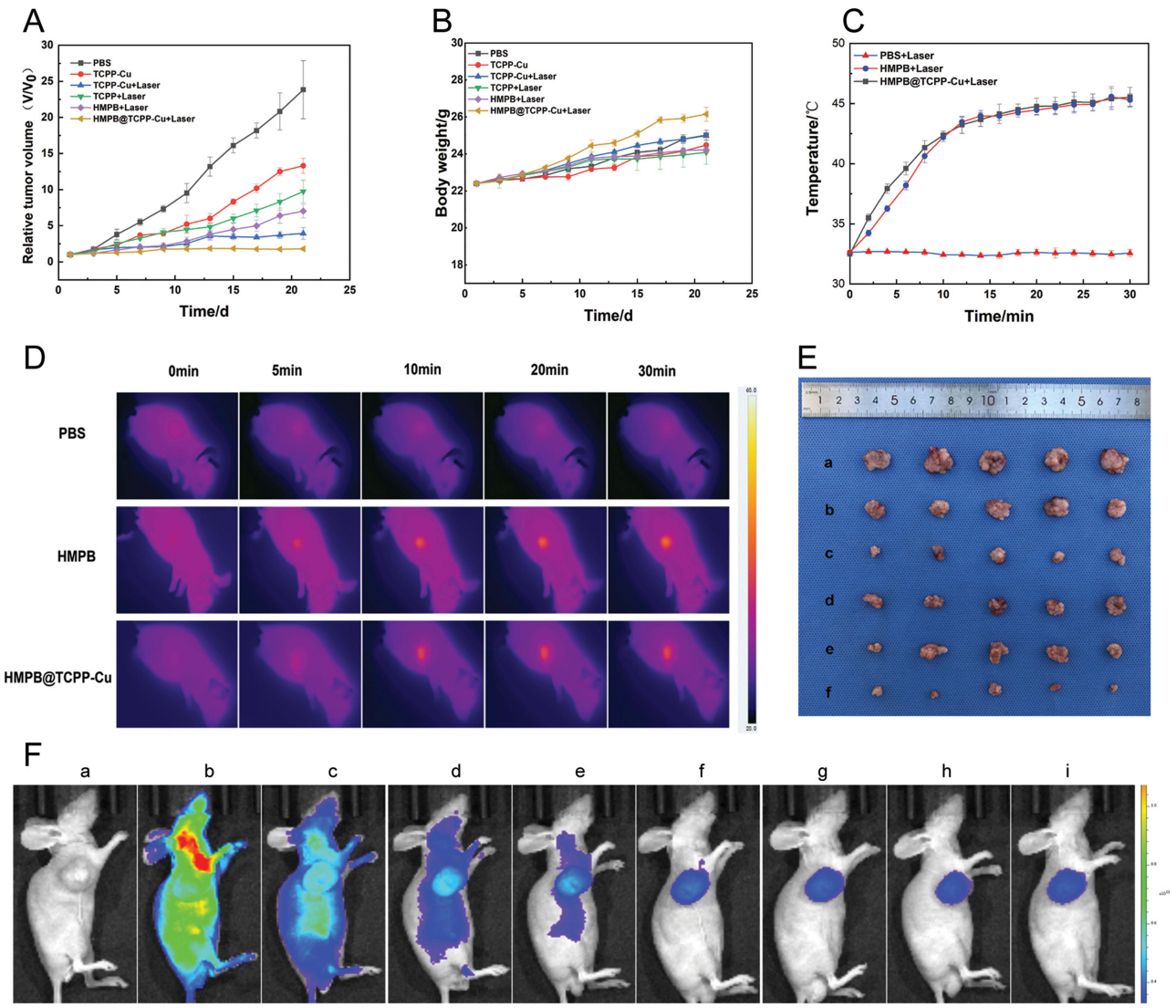

Figure 4 In vivo anti-tumor studies (**A**) Curves showing the time-course changes in the subcutaneous tumor volume of the nude mice in each experimental group after treatment. (**B**) The changes in the body weight of the nude mice in each experimental group after treatment. (**C**) Curves showing the temperature change in the body surface of the nude mice under laser irradiation, as recorded using a thermal infrared camera. (**D**) Thermal images of the body surfaces of the nude mice during laser irradiation, as recorded using a thermal infrared camera. (**E**) Appearance of the subcutaneous tumors isolated from the nude mice: a. PBS; b. TCPP-Cu; c. TCPP-Cu+Laser; d. TCPP+Laser; e. HMPB+Laser; f. HMPB@TCPP-Cu+Laser. (**F**) Biodistribution of the HMPB@TCPP-Cu nanoparticles.

hyperthermia-mediated PTT. In comparison, the temperature of the PBS group only increased slightly (Figure 4C and D). This result shows that the therapeutic effect of PTT was achieved upon laser irradiation by inducing apoptosis in tumor cells, subsequently inhibiting tumor growth.

Biodistribution of the HMPB@TCPP-Cu Nanoparticles

The HMPB@TCPP-Cu nanoparticles were labeled with Cy5.5 and injected into HuH6 tumor-bearing nude mice via the tail vein to observe their biodistribution. At fixed time points after tail vein injection, the distribution of HMPB@TCPP-Cu was tracked by imaging the mice in the in vivo imaging system IVIS. The fluorescence intensity of the particles in the tumor tissues gradually increased with time and reached higher intensities at 12–24h after HMPB@TCPP-Cu injection. This indicates that the distribution of HMPB@TCPP-Cu is time-dependent, which may be due to the EPR (enhanced permeability and retention) effect of tumors (Figure 4F).

Evaluation of the Apoptosis Mechanisms in vivo

Each group of nude mice received the corresponding drug via the tail vein and was subjected to laser irradiation for three treatment cycles. Twenty-four hours after the end of the treatment, the mice were anesthetized and then sampled by sectioning the tumor tissues from each experimental group and staining the sections for caspase-3 and caspase-9. The most pronounced expression of caspase-3 and caspase-9, characterized by strong brown staining of the cytoplasm, was observed in the HMPB@TCPP-Cu+Laser group. In contrast, the control group showed much lower expression levels, consistent with the TUNEL and HE staining results. Apoptosis is characterized by the expression of caspase-9 followed by functional cleavage of caspase-3 (Figure 5A and B). Thus, the overexpression of caspase-9 and caspase-3 in the HMPB@TCPP-Cu+Laser group suggests that the apoptosis of tumor cells upon treatment with HMPB@TCPP-Cu and laser irradiation was mediated by the caspase pathway. The tumor tissues were also sectioned and stained for PCNA. The staining results showed that Group 6 had the lowest cell proliferation activity, while Group 1 had the highest proliferation activity; the other experimental groups had intermediate levels. These results indicate that the nanoparticles in this study have an inhibitory effect on the proliferation of tumor tissues and that the effects of multiple therapeutic approaches were synergistically amplified (Figure 5C).

Evaluation of Heat Shock Protein Production

To further explore the mechanism underlying the synergistic effects of the various therapies, 24 h after the end of three treatment cycles, immunofluorescence staining for HSP70 and HSP90 was performed to investigate the inhibitory effect of these ROS-generating therapies on the expression of heat-resistant proteins. The levels of heat shock proteins in Group 6 were the lowest among all groups, while the highest levels were found in Group 5; the remaining four groups showed intermediate levels (Figure 5E and F). This shows that the ROS produced by PDT and CDT can inhibit the production of heat shock proteins, thus reducing or even eliminating the heat resistance of tumor cells to the long-standing effect of PTT.

The tumor tissue sections were also stained for Hif-1α. The staining results showed that because HMPB has peroxidase-like activity, it provides a reactive substrate for photodynamic therapy and chemodynamic therapy, alleviating the oxygen deficiency caused by ROS generation (Figure 5D).

Assessment of ROS Production

After each group of nude mice received the corresponding drug and was treated with laser irradiation, the mice were anesthetized and sampled within 30 min. The tumor tissues were then immediately preserved using liquid nitrogen and assayed for ROS production. The results of the ROS content assay revealed that Group 6 had the highest ROS content, which was inextricably linked to the effect of PDT, CDT, and the increase in temperature mediated by PTT, all of which enhanced ROS production. The ROS content in Groups 1 and 5 was relatively low, which was related to the fact that no ROS was produced in these two groups (Figure 5G).

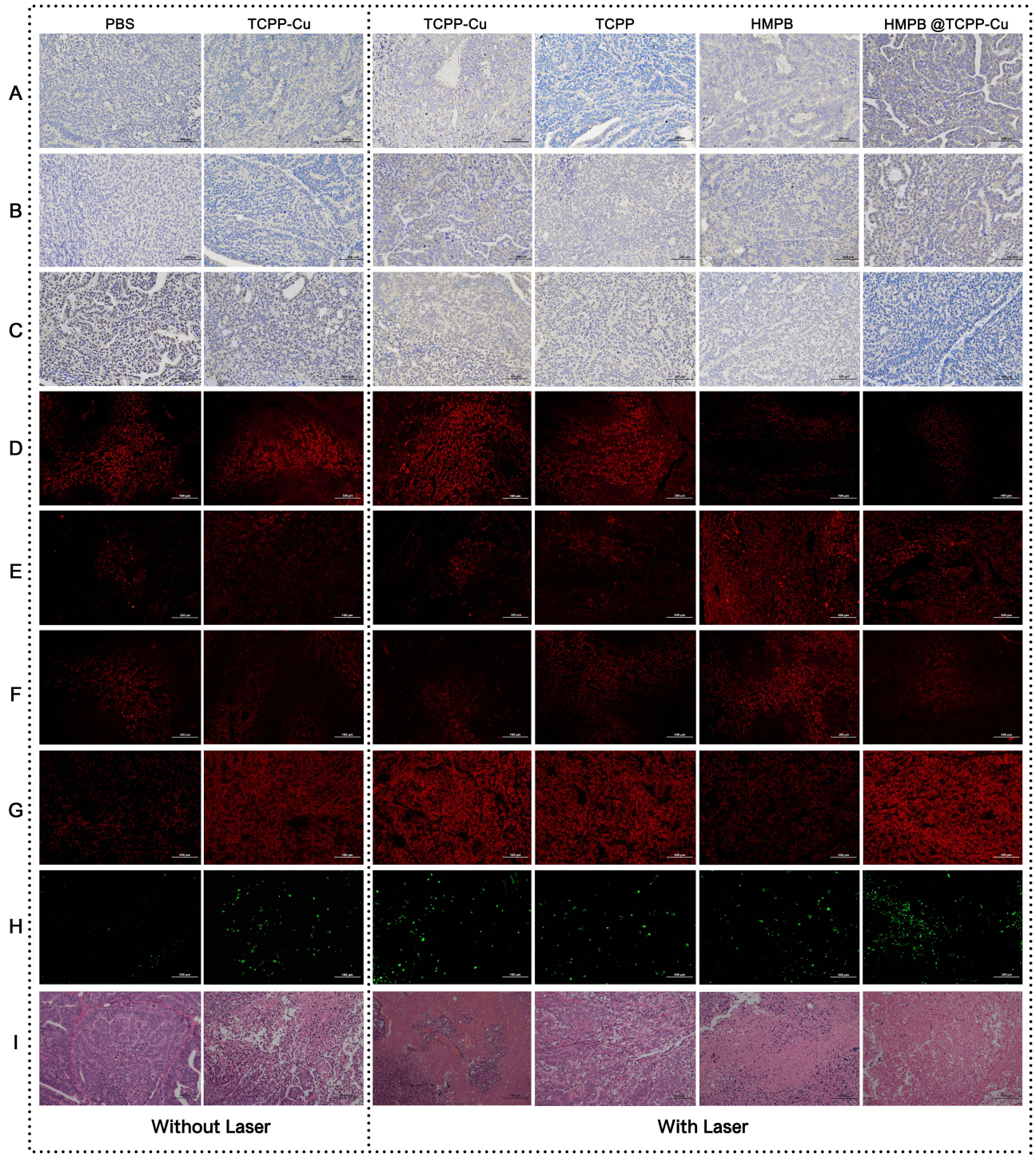

Figure 5 Representative images of stained tumor tissue sections of nude mice after treatment in each experimental group. Each set of images was stained for (**A**) caspase-3, (**B**) caspase-9, (**C**) PCNA, (**D**) HIF-1α, (**E**) HSP70, (**F**) HSP90, (**G**) ROS, (**H**) TUNEL assay, and (**I**) HE.

Evaluation of Apoptosis in vivo

Each group of nude mice received the corresponding drug injected into the tail vein and was subjected to laser irradiation for three treatment cycles. Twenty-four hours after the end of treatment, the nude mice were anesthetized and sampled. HE and TUNEL staining were then performed on the tissue sections obtained from each mouse. The results showed that the tumor cells in Group 1 grew well; compared to Group 1, the tumor tissue in Group 6 showed significant apoptosis. Moreover, the other groups also showed different degrees of apoptosis, as shown in the photographic images of the stained tissues (Figure 5H and I).

Tumor tissues were also isolated, sectioned, and stained to evaluate cell proliferation. It can be seen that the tumor cells in the Group 6 were in the worst state, those in Group 1 had the best growth state, and the rest of the groups exhibited varying degrees of growth inhibition (Figure 5H and I). In summary, the nanomaterial-mediated apoptosis of tumor cells was achieved, and there is a certain degree of synergistic effect between the treatment modalities.

Biotoxicity Testing of the Nanoparticles in vivo

The heart, lung, spleen, liver, and kidney tissues of the nude mice were sectioned after formaldehyde fixation, and the tissue sections were stained with HE. The results showed no significant difference between each organ of the experimental group of nude mice compared with the control group (Figure S19). These results show that the novel nanoparticles synthesized in this experiment were biologically safe.

Taken together, our results confirm the synergistic effects induced by an all-in-one therapeutic modality mediated by HMPB@TCPP-Cu.

Conclusions

In this study, the formulation of nanoplatform was successfully optimized, and a novel multifunctional nanoparticle composite, HMPB@TCPP-Cu, was synthesized. This composite significantly improved the tumor microenvironment, exhibiting enhanced capabilities in photothermal therapy, photodynamic therapy, and chemodynamic therapy. With oxygen generation and ROS production, the goal on the cleavage of HSPs and the coupling thermal resistance was achieved, leading to suppressed tumor growth and satisfied therapeutic efficacy. This study presents a multifunctional nanoplatform for efficient hepatoblastoma treatment via modulating ROS and HSPs. Collectively, this study provides an appealing strategy in the cleavage of thermal resistance and a novel assistance and enhancement on thermal-related therapies.

Data Sharing Statement

All data generated and analyzed in this study are available by reasonable request of the corresponding author.

Ethics Approval and Consent to Participate

The experiments were approved by the Ethical Committee of Shandong Provincial Hospital (No. 2022-039).

Funding

This study was supported by grants from the Shandong First Medical University (Shandong Academy of Medical Sciences) Youth Science Foundation Incubation Grant Program (No.202201-051); Innovation Pilot Project of Integration of Science, Education and Industry of Qilu University of Technology (Shandong Academy of Science) (No. 2022PX098); National Natural Science Foundation of China (82102040); Natural Science Foundation of Shandong Province (ZR2021QH228); Taishan Scholars Program of Shandong Province (tsqnz20221171); Shandong Province Science and Technology Development Plan (No.003130113).

Disclosure

The authors report no conflicts of interest in this work.

References

1. Sharma D, Subbarao G, Saxena R. Hepatoblastoma. *Semin Diagn Pathol*. 2017;34(2):192–200. doi:10.1053/j.semdp.2016.12.015
2. Waters AM, Mathis MS, Beierle EA, Russell RT. A synopsis of pediatric patients with hepatoblastoma and Wilms tumor: NSQIP-P 2012–2016. *J Surg Res*. 2019;244:338–342. doi:10.1016/j.jss.2019.06.064
3. Zhi D, Yang T, O'Hagan J, Zhang S, Donnelly RF. Photothermal therapy. *J Control Release*. 2020;325:52–71. doi:10.1016/j.jconrel.2020.06.032
4. Li C, Cheng Y, Li D, et al. Antitumor applications of photothermal agents and photothermal synergistic therapies. *Int J Mol Sci*. 2022;23(14):7909.
5. Xin Y, Sun Z, Liu J, et al. Nanomaterial-mediated low-temperature photothermal therapy via heat shock protein inhibition. *Front Bioeng Biotechnol*. 2022;10:1027468. doi:10.3389/fbioe.2022.1027468
6. Ali MR, Ali HR, Rankin CR, El-Sayed MA. Targeting heat shock protein 70 using gold nanorods enhances cancer cell apoptosis in low dose plasmonic photothermal therapy. *Biomaterials*. 2016;102:1–8. doi:10.1016/j.biomaterials.2016.06.017

7. Xia Y, Li C, Cao J, et al. Liposome-templated gold nanoparticles for precisely temperature-controlled photothermal therapy based on heat shock protein expression. *Colloids Surf B Biointerfaces*. 2022;217:112686. doi:10.1016/j.colsurfb.2022.112686
8. Wang S, Tian Y, Tian W, et al. Selectively sensitizing malignant cells to photothermal therapy using a CD44-targeting heat shock protein 72 depletion nanosystem. *ACS Nano*. 2016;10(9):8578–8590. doi:10.1021/acsnano.6b03874
9. Cramer GM, Cengel KA, Busch TM. Forging forward in photodynamic therapy. *Cancer Res*. 2022;82(4):534–536. doi:10.1158/0008-5472.CAN-21-4122
10. Lan M, Zhao S, Liu W, Lee CS, Zhang W, Wang P. Photosensitizers for photodynamic therapy. *Adv Healthc Mater*. 2019;8(13):e1900132. doi:10.1002/adhm.201900132
11. Zhao P, Li H, Bu W. A forward vision for chemodynamic therapy: issues and opportunities. *Angew Chem Int Ed Engl*. 2023;62(7):e202210415. doi:10.1002/anie.202210415
12. Anderson NM, Simon MC. The tumor microenvironment. *Curr Biol*. 2020;30(16):R921–R925. doi:10.1016/j.cub.2020.06.081
13. Petrova V, Annicchiarico-Petruzzelli M, Melino G, Amelio I. The hypoxic tumour microenvironment. *Oncogenesis*. 2018;7(1):10. doi:10.1038/s41389-017-0011-9
14. Li Y, Zhao L, Li X-F. Hypoxia and the Tumor Microenvironment. *Technol Cancer Res Treat*. 2021;20:15330338211036304. doi:10.1177/15330338211036304
15. Cui T, Li X, Shu Y, Huang X, Wang Y, Zhang W. Utilizing glutathione-triggered nanoparticles to enhance chemotherapy of lung cancer by reprograming the tumor microenvironment. *Int J Pharm*. 2018;552(1–2):16–26. doi:10.1016/j.ijpharm.2018.09.050
16. Zhang ZJ, Wang KP, Mo JG, Xiong L, Wen Y. Photodynamic therapy regulates fate of cancer stem cells through reactive oxygen species. *World J Stem Cells*. 2020;12(7):562–584. doi:10.4252/wjsc.v12.i7.562
17. Yuan B, Wang H, Xu JF, Zhang X. Activatable photosensitizer for smart photodynamic therapy triggered by reactive oxygen species in tumor cells. *ACS Appl Mater Interfaces*. 2020;12(24):26982–26990. doi:10.1021/acsami.0c07471
18. Wang T, Xu X, Zhang K. Nanotechnology-enabled chemodynamic therapy and immunotherapy. *Curr Cancer Drug Targets*. 2021;21(7):545–557. doi:10.2174/1568009621666210219101552
19. Chen Q, Li N, Wang X, et al. Mitochondria-targeting chemodynamic therapy nanodrugs for cancer treatment. *Front Pharmacol*. 2022;13:847048. doi:10.3389/fphar.2022.847048
20. Wang J, Kong W, Jin H, et al. Tumor microenvironment responsive theranostic agent for enhanced chemo/chemodynamic/photothermal therapy. *Colloids Surf B Biointerfaces*. 2022;218:112750. doi:10.1016/j.colsurfb.2022.112750
21. Tang H, Li C, Zhang Y, et al. Targeted Manganese doped silica nano GSH-cleaner for treatment of Liver Cancer by destroying the intracellular redox homeostasis. *Theranostics*. 2020;10(21):9865–9887. doi:10.7150/thno.46771
22. Zhong D, Wang Y, Xie F, et al. A biomineralized Prussian blue nanotherapeutic for enhanced cancer photothermal therapy. *J Mater Chem B*. 2022;10(25):4889–4896. doi:10.1039/D2TB00775D
23. Dong H, Wang G, Feng K, et al. Reference material of Prussian blue nanozymes for their peroxidase-like activity. *Analyst*. 2022;147(24):5633–5642. doi:10.1039/D2AN01401G
24. Cui R, Li B, Liao C, Zhang S. Copper-mediated chemodynamic therapy with ultra-low copper consumption by doping cupric ion on cross-linked (R)-(+)-lipoic acid nanoparticles. *Regen Biomater*. 2023;10:rbad021. doi:10.1093/rb/rbad021
25. Liu L, Zhang H, Peng L, et al. A copper-metal organic framework enhances the photothermal and chemodynamic properties of polydopamine for melanoma therapy. *Acta Biomater*. 2023;158:660–672. doi:10.1016/j.actbio.2023.01.010
26. Hu C, Cai L, Liu S, Liu Y, Zhou Y, Pang M. Copper-doped nanoscale covalent organic polymer for augmented photo/chemodynamic synergistic therapy and immunotherapy. *Bioconjug Chem*. 2020;31(6):1661–1670. doi:10.1021/acs.bioconjchem.0c00209
27. Yang J, Yang L, Li Q, Zhang L. Ferrocene-based multifunctional nanoparticles for combined chemo/chemodynamic/photothermal therapy. *J Colloid Interface Sci*. 2022;626:719–728. doi:10.1016/j.jcis.2022.06.117
28. He R, Zang J, Zhao Y, et al. Nanofactory for metabolic and chemodynamic therapy: pro-tumor lactate trapping and anti-tumor ROS transition. *J Nanobiotechnology*. 2021;19(1):426. doi:10.1186/s12951-021-01169-9